energies

Article

Numerical Analysis of E-Machine Cooling Using Phase Change Material

Jayakumar Selvan [1] and Sreekanth Manavalla [1,2,*]

[1] School of Mechanical Engineering, Vellore Institute of Technology Chennai, Chennai 600127, India; jayakumar.selvan2018@vitstudent.ac.in
[2] Electric Vehicles Incubation, Testing and Research Centre, Vellore Institute of Technology Chennai, Chennai 600127, India
* Correspondence: manavalla.sreekanth@vit.ac.in

Abstract: The cooling of E-machines was investigated using phase change material (PCM). The PCM is widely used in the cooling of electronic components because of its heat-absorbing and cooling properties. In this study, PCM OM35 (50:50) and OM35 (60:40) were used for the cooling of E-Machines, which are commonly known as electric vehicle motors. Three different configurations, viz. no rib, two ribs, and four ribs, were studied to understand the impact of thermal behaviour on bracket cooling. The ribs were added in between the brackets to enhance the heat transfer. Numerical simulations were performed using the volume of fluid multiphase analysis approach to model the behaviour of phase change inside the brackets for 18 KW E-Machines. Based on the study, a four rib configuration showed good performance compared to no rib and two rib configurations, and heat transfer improved by 6%. Heat transfer is thus improved by increasing the number of ribs placed between the brackets. The cyclic heat load was applied to the best performing ribs to study the impact of different PCM materials OM35 (50:50) and OM35 (60:40).

Keywords: multi phase analysis; ribs; E-Machines; phase change materials (PCM); computational fluid dynamics (CFD)

Citation: Selvan, J.; Manavalla, S. Numerical Analysis of E-Machine Cooling Using Phase Change Material. *Energies* **2022**, *15*, 5594. https://doi.org/10.3390/en15155594

Academic Editors: Eric Cheng and Junfeng Liu

Received: 2 June 2022
Accepted: 15 July 2022
Published: 2 August 2022

1. Introduction

Strict operating specifications apply to electric machines designed for traction purposes. Traction E-machines with excessive energy density and mechanical robustness require a broad range of operation and higher performance. They are designed to deliver high torque at low velocities and high cruising power. The E-machines are built with strict thermal specifications owing to the conditions of intense loading.

Many previous researchers and designers have traditionally followed a thermal network model for electrical driven machines under constant and intermittent thermal conditions Mellor et al. 1991 [1]. One of the popular numerical techniques is the finite difference method. While this methodology forecasts hot spot temperatures, the approach to dealing with complicated boundary conditions and geometry is no longer as robust as the finite volume approach. In recent years, the use of the finite volume technique for thermal induction E-machine evaluation has gained wide acceptance among researchers and its evolution is shown in Figure 1. Several investigators have experimented to examine the effect of a given design and to validate the theoretical and numerical concept of electrical machines.

The primary purpose for electric driven E-machines is to transform electrical energy input into mechanical power output. Therefore, a model that represents the dynamic relation between the electromagnetic torque and the electric inputs is desired. In vehicle applications, there are a variety of engines that can be used.

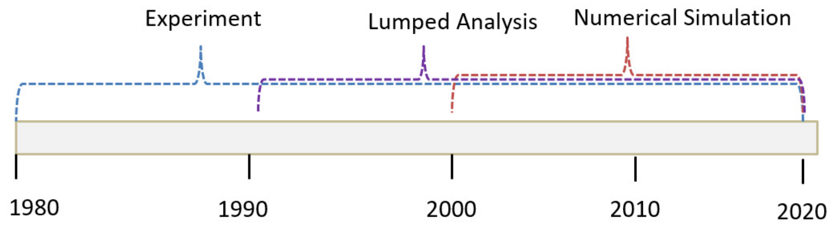

Figure 1. Evolution of thermal analysis.

E-machines have significant advantage compared to the traditional internal combustion engine: (i) High density of force and amplitude of torque two times higher than IC engines, (ii) Large ranges of speeds with constant processing power about three to four times the rated speed, (iii) High starting torque, fast climbing and cruising speed, (iv) High performance over large ranges of speeds and torques, (v) High reliability and environmental friendliness and (vi) Minimal acoustic noise.

Under extreme temperature conditions, traction E-machines are still required to work reliably. In addition, permanent magnets generally used in traction E-machines are highly temperature sensitive. Thermal management is therefore an integral element in the design of E-machines, but thermal modelling can be a complicated issue. Airflow awareness in a motor is crucial for design applications, in particular when heat transfer limits for airflow convection are exceeded. The convective heat transfer coefficients are necessary to measure temperatures which depend on geometry and fluid flow. Huan et al. [2] have studied the organic phase change material with two different types of housing. The studies were compared with experimental results and found to have a good correlation with numerical results. The impact between the metal housing and acrylic housings was studied. M. Sheikholeslami et al. [3] have studied the impact of fins and nanoparticles on the heat exchanger system and the nanoparticles improve the performance.

Matsuzakieta et al. [4] investigated the use of gas for motor cooling. Davin et al. [5] investigated the oil cooling for the motors and also studied the different types of injection patterns to improve heat transfer. Limand et al. [6] studied the different oil cooling methods used in electrical vehicles. King et al. [7] and Kim et al. [8] studied different cooling passages used for the electrical motors. Huangetal [9] describes how to use the oil cooling system to reduce the operating temperature of the motor. Mudawar et al. [10] proposed oil spraying methods for cooling the motors. Karim and Yus [11] investigated the liquid cooling method to enhance the heat transfer. Zhang et al. [12] studied air and liquid cooling to control the temperature behaviour using a mathematical model.

Camilleri et al. [13] investigated the evaporative cooling system for the rotor assembly. This paper explained the importance of combined cooling to achieve the cooling requirements. Woolmer et al. [14] studied the yokeless motor and found it increased the torque density and overall performance of the motor. Lamperth et al. [15] developed technology based on axial flux topology. This technology offers better performance because of its increased area for cooling. Liwei et al. [16] discussed motor performance and its impact on the temperature field, drawing some important conclusions about motor cooling. Yoon et al. [17] studied the fan performance for the optimum efficiency of the motor, and further study was conducted on several cooling methods and their impacts on the fan performance efficiency. Odvářka et al. [18] numerically evaluated the cooling performance of the permanent magnet machine under different flow rates and operating conditions and compared it with analytical results. Brütsch et al. [19] investigated the impact of insulation failure, which is again subdivided into other categories of failure. Emanuel et al. [20] shared some observations on voltage distortion and thermal ageing.

The OM35 and paraffin combination is used for this numerical simulation. It consists of straight-chain hydrocarbons and is environmentally friendly. It does not create any hazardous situations when it is combined with other materials such as aluminium. The combination of OM35 and paraffin with two different mixing percentages was used for this study, 50:50 and 60:40. These mixing combinations aid in achieving the desired melting point for low voltage applications.

The PCM has not been studied extensively as an alternative cooling medium for E-machine. To understand the shortcomings and advantages of the PCM as coolant. This paper examines PCM OM35 use as coolant for cooling the stator and brackets. The OM35 is used as coolant because it has a melting temperature of 35 °C. The objective of this is to understand whether the PCM can be used for cooling the E machine and check whether this can be an alternative to the liquid cooling system. Based on the literature survey so far, the research carried out on E-machine is based on a liquid cooling system. Nowhere is PCM studied extensively for cooling motors. So, in this project, the PCM is provided in the main flow passage to enable an increased heat transfer efficiency.

The research design is to optimize the design of the PCM cooling circuit as shown in Figure 2. As of now, there are only a few research papers available on liquid and PCM cooling on E-Machines. The sections below explain the process that was used to carry out the PCM simulation.

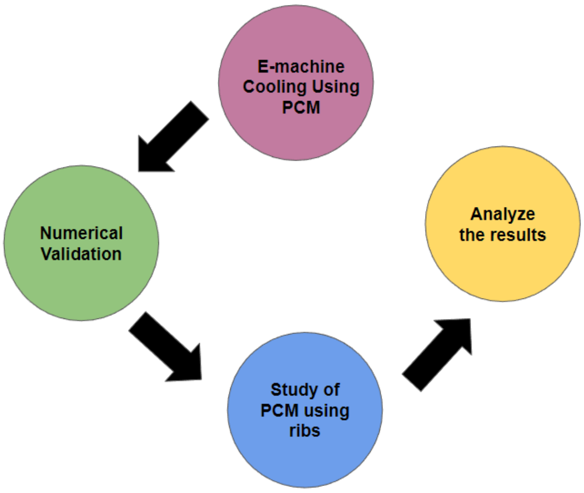

Figure 2. Research design of thermal analysis.

2. Geometry

The cooling study was conducted using a simplified CAD model of the E-Machine as shown in the figure. The E-Machine consists of an inner, outer bracket, and a stator as shown in Figure 3 [21,22]. The stator stack is the place where the heat source of 18 KW is applied. The PCM OM35 is filled between the inner and outer brackets. The geometry parameters of the E-machine are shown in the below Table 1. Three configurations are studied in the paper to improve the heat transfer using PCM; they are no rib, two rib, and four rib configurations. The ribs were placed equally in the axial direction as shown in Figure 4. The outer bracket is applied with a convective heat transfer of 10 W/m^2-K and the latent heat of PCM considered for PCM is 250 kJ/kg. The other walls were treated as adiabatic as shown in Figure 5. To monitor the phase change of PCM, the plane section is created as shown in the Figure 6 and the melting process is monitored for every time step till it reaches 100 s.

Table 1. Dimensions of E Machine.

Geometric Parameter	Cooling Jacket	Electric Motor
Length	163 mm	210 mm
Thickness	10 mm	50 mm

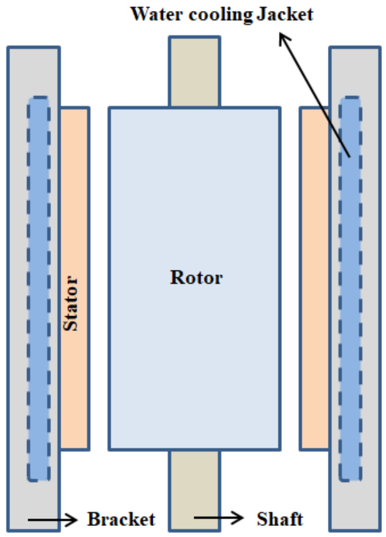

Figure 3. Symmetric diagram of E-Machine.

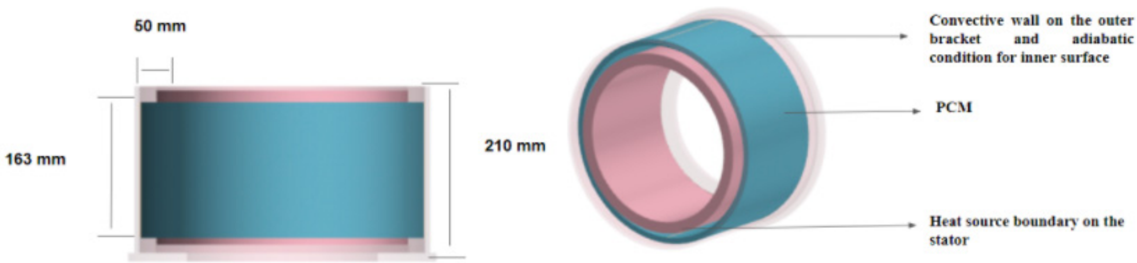

Figure 4. Boundary Definition of E-Machine.

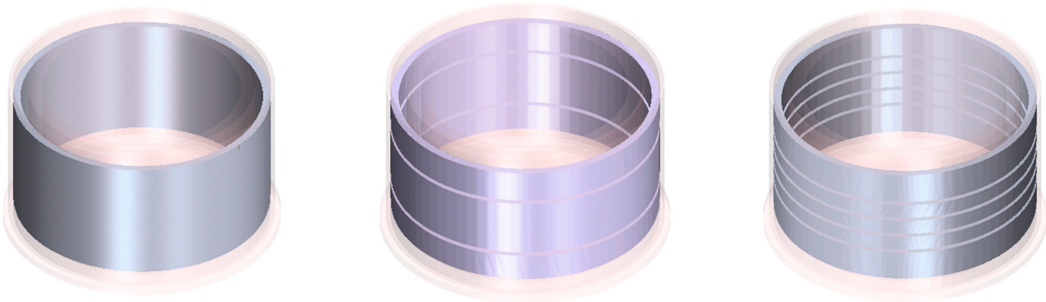

(**a**) No Rib Configuration (**b**) Two Rib Configuration (**c**) Four Rib Configuration

Figure 5. Different type of rib configurations used in the study.

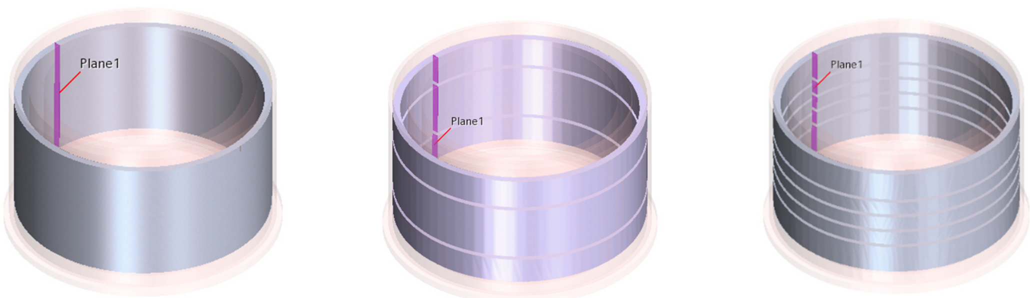

(**a**) No Rib Configuration (**b**) Two Rib Configuration (**c**) Four Rib Configuration

Figure 6. Plane section location to monitor the phase change.

3. Melting and Solidification

The process of melting converts material from a solid to a liquid state, when a solid material is heated to the melting point. Solidification is the reverse process. When it comes to pure substances like water, the liquidus and the solidus are often at the same temperature when melting and solidifying occur. The liquid-solid interface is not explicitly tracked by the melting-solidification model used in Simcenter STAR-CCM+. The distribution of the liquid-solid phase's solidified component is instead determined by the model using an enthalpy formulation.

For melting-solidification, the enthalpy of the liquid-solid phase h_{ls} includes the latent heat of fusion h_{fusion}

$$h_{ls}{}^{*} = h_{ls} + (1- \propto^{*})\, h_{fusion}$$

where h_{ls} is the sensible enthalpy.

The relative solid volume fraction $\propto^{*}$ is defined as the portion of the volume of the liquid-solid phase that is in the solid state. In the enthalpy model, the relative solid volume fraction $\propto^{*}$ is a function of temperature:

$$\propto^{*} = \begin{cases} 1, \mathrm{T}^{*} < 0 \\ f(\mathrm{T}), 0 < \mathrm{T}^{*} < 1 \\ 0, 1 < \mathrm{T}^{*} \end{cases}$$

where T^{*} is the normalized temperature that is defined as:

$$\mathrm{T}^{*} = \frac{T - T_{solidus}}{T_{liquidus} - T_{solidus}}$$

The function $\mathrm{f(T)}$ is called the fraction solid curve. For a linear dependence between $\propto^{*}$ and T^{*}, the solidification path is defined as:

$$\mathrm{f(T)} = 1 - \mathrm{T}^{*}$$

In addition, it is also possible to provide the solidification path as a table, in which case linear relationships are taken into account between the points in the table. The relative solid fraction values in the table must drop monotonically while the temperature values must rise monotonically.

A linear solidification path is assumed and a small temperature interval of 0.002 K is automatically introduced if melting and solidification occur at the same temperature. The liquid-solid phase's physical characteristics may be constant or may depend on temperature and the relative volume proportion of solids.

RANS Turbulence Models

The Reynolds-Averaged Navier–Stokes equations, which control the transfer of the mean flow quantities, are closed by the RANS turbulence models.

Each solution variable in the instantaneous Navier–Stokes equations is divided into its mean ϕ, or averaged, value ϕ^{-} and its fluctuating component ϕ' to produce the Reynolds-Averaged Navier–Stokes equations.

$$\phi = \phi^{-} + \phi'$$

Over a finite control volume mass, momentum, and energy transport equations can be written as:

$$\frac{\partial}{\partial \mathrm{t}} \int_{\mathrm{V}} \rho_{\mathrm{i}} \mathrm{dV} + \int_{\mathrm{A}} \rho_{\mathrm{i}} \mathrm{V} \cdot \mathrm{da} = \int S_u dV$$

$$\frac{\partial}{\partial \mathrm{t}} \int_{\mathrm{V}} \rho_{\mathrm{i}} \mathrm{V} \mathrm{dV} + \int_{\mathrm{A}} \rho_{\mathrm{i}} \mathrm{V} \cdot \mathrm{V} \mathrm{da} = - \int p\, I \cdot da + \int_{\mathrm{V}} f_b \mathrm{dV} + \int_{\mathrm{V}} S_u\, dV$$

where t is time., V is volume, a is the area vector, ρ is the density, v is the velocity, p is pressure, f_b is the resultant of body forces, S_u is a user-specified source term.

Heat transfer is the exchange of thermal energy across mediums at different temperatures. In order to reach an equilibrium state the heat transfer happens from higher to lower temperatures. Heat transfer can be calculated within a fluid (single or multi-component), between different fluid streams, between a fluid and a solid, and within a solid.

The governing equation for the transfer of energy within a fluid

$$\frac{\partial}{\partial t}\int_{V} \rho_i E dV + \int_{A} \rho_i H \cdot v da = \int_{V} q \cdot da + \int_{A} \Sigma h_i J_i da + \int_{V} S_u \, dV$$

The governing equation for the transfer of energy within a solid

$$\frac{\partial}{\partial t}\int_{V} \rho \, C_p T \, dV + \int_{A} \rho \, C_p T \, V_s da = \int_{V} q \cdot da + \int_{V} S_u \, dV$$

where, ρ is the solid density, C_p is the specific heat, T is the temperature, q is the heat flux vector, E is the total energy, H is the total enthalpy, h_i is the enthalpy of component I, J_i is the diffusive flux of component I, S_u is a user-specified source term, v_s is the solid convective velocity (only applicable when the region is a pure body of rotation).

4. Experimental Validation with CFD

The numerical validation with experimental data will help us to confirm that the results are independent of mesh and solver parameters. In this study, the numerical validation is performed by comparing the results published by Pradeep [23]. A very similar domain is considered, and the cases were compared for similar boundary conditions. The outer boundary was kept as adiabatic and copper plate was applied with 1,120,000 W/m^3. From the results, the temperature measurement across different probe points T1,T2,T3 & T4 was compared with CFD results and found to have good correction with experiment as shown in Figure 7 and Table 2. The PCM phase transformation for 1800 s was compared with the experiment and found to have a similar trend. Based on the correlation, the solver settings were selected and used for further analysis.

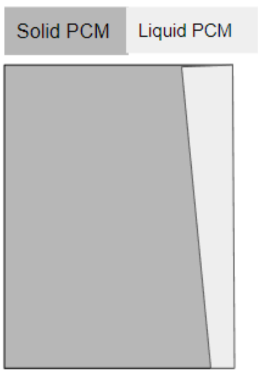

(**a**) Experimental Time =1800 s

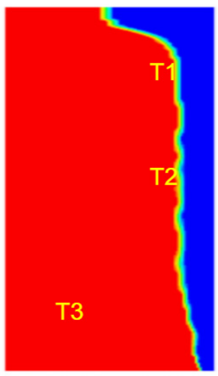

(**b**) CFD Time =1800 s

Figure 7. Comparison between the CFD and Experimental [23] data.

Table 2. Validated results between the CFD and Experimental [23].

Probe Point	Experimental	CFD
T1	55 °C	57 °C
T2	-	50 °C
T3	-	25 °C

Solution Independent Studies

The bracket temperature was monitored for the different time steps in order to find the time step which is independent of the solution. Based on the study, the solution was found to be independent of the results after 0.002 s. The mesh independence study was also investigated to eliminate the impact of element size on the solution. Around seven million polyhedral cells were found to be ideal for the cooling system to be independent of results as shown in Figures 8 and 9.

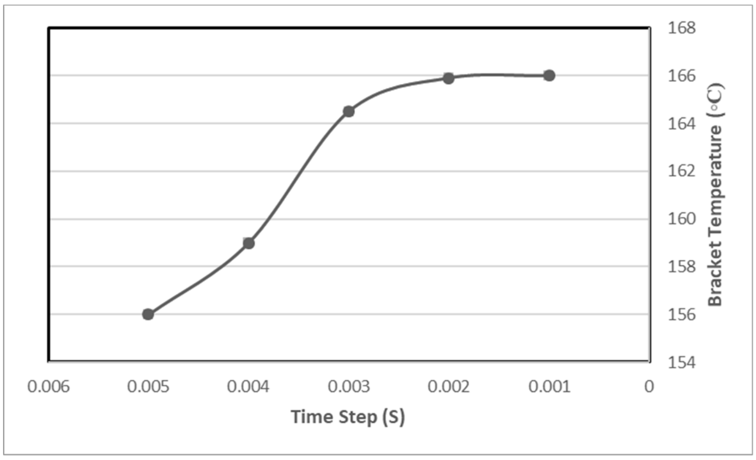

(**a**) Time step study

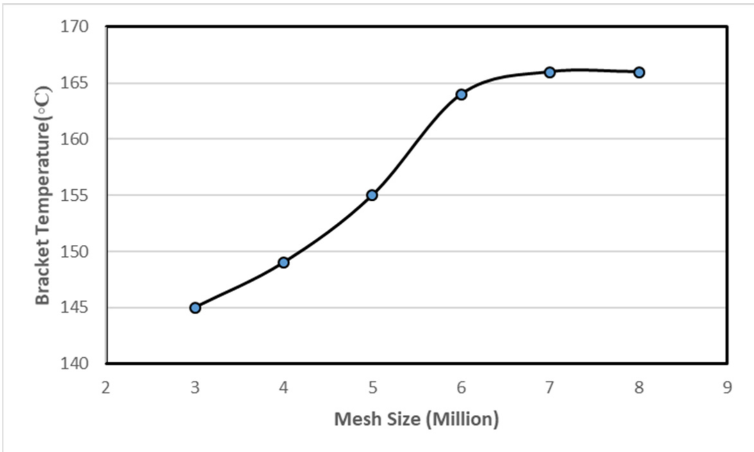

(**b**) Grid independence study

Figure 8. Solution independent studies.

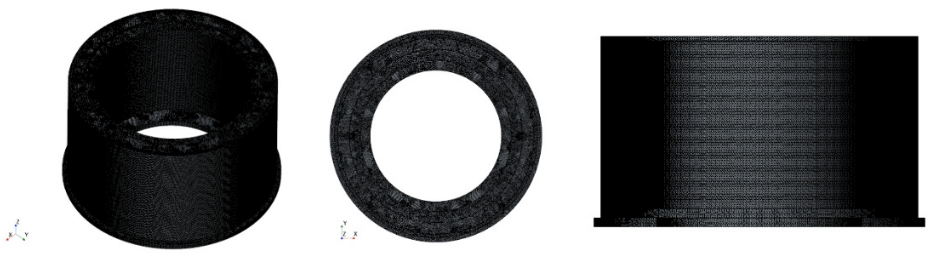

Figure 9. Different views of polyhedral mesh.

5. Solver Settings

The simulation was performed using a multiphase with phase interaction model. The Eulerian multiphase model was used to capture the phase transformation from solid to liquid, which is based on the control volume approach. The melting and solidification model in STAR-CCM+ is used to track the enthalpy formulation, which helps to determine the solid portion of the liquid-to-solid interface. The K Epsilon turbulence model was used to capture the fluid flow behaviour of the liquid phase of the PCM. The implicit unsteady state simulation was performed for a total time step of 100 s. The material properties of the PCM OM35 are shown in the below Table 3. The continuity, momentum, turbulence, and energy equations were monitored for convergence with criteria of residual below 1×10^{-1}. In addition, the volume fraction of PCM and temperature were also monitored for convergence.

Table 3. Material properties of Phase change material.

Properties	OM35 (50:50)	OM35 (60:50)
Melting temperature (°C)	46.5	52.4
Density–Solid (kg/m^3)	740	740
Density–liquid (kg/m^3)	709.5	701.6
Specific heat—(J/kg·K)	1650	1620
Specific heat—(J/kg·K)	2219	2182
Thermal conductivity—(W/m·K)	0.17	0.156
Viscosity—(kg/m·s)	0.01602	0.01563

6. Results and Discussion

The detailed impact on the thermal behavior of the E-machine is covered under two topics. The first topic explains the volume change as a function of time with a heat source, and the second topic covers the temperature behavior of brackets as a function of time with a heat source. Volume change and thermal behavior are discussed for all three configurations.

6.1. Comparison of Volume Change for Different Rib Configuration

In Figure 10, the y axis shows the percentage of volume fraction of PCM that changes with respect to time. It is clear that there is no percentage of volume change for a time period of 10 s. After 10 s, the volume change of the PCM starts. The volume change of PCM starts when the temperature of PCM increases by roughly 5 °C. The PCM remains about 98% solid while 2% is converted into liquid at the time of 10 s. After 10 s, four rib configurations seem to change the phases of PCM faster when compared to no rib and two rib configurations. At 30 s, 10% of PCM in four rib configurations was converted into liquid, whereas only 6.7% and 7.0% of PCM were converted into liquid in other configurations. For an increase in temperature of 25 °C, the four rib configurations seem to perform better for the cooling. Until 30 s, the two rib configurations appear to perform similarly. But after 30 s, the four and two rib configurations seem to melt the PCM faster when compared to no rib configurations. The four rib configurations melt the PCM by 5%, which is higher than the two rib configurations and 10% by no rib configurations. After 100 s, 55% of the PCM is melted into liquid, while 45% remains solid in four rib configurations, 50% in two rib configurations, and 60% in no rib configurations.

The melting process is very slow with no rib configurations as shown in the Figure 11. There is no significant change in the phase of material till 20 s. After 20 s, there is some small change in PCM. It continues till 100 s, where the PCM changes the phase by 40%. The same behaviour can be observed in the inner and outer brackets. The heat transfer from the outer bracket to the surroundings is limited because PCM with no rib configurations takes more time to absorb heat from the inner brackets.

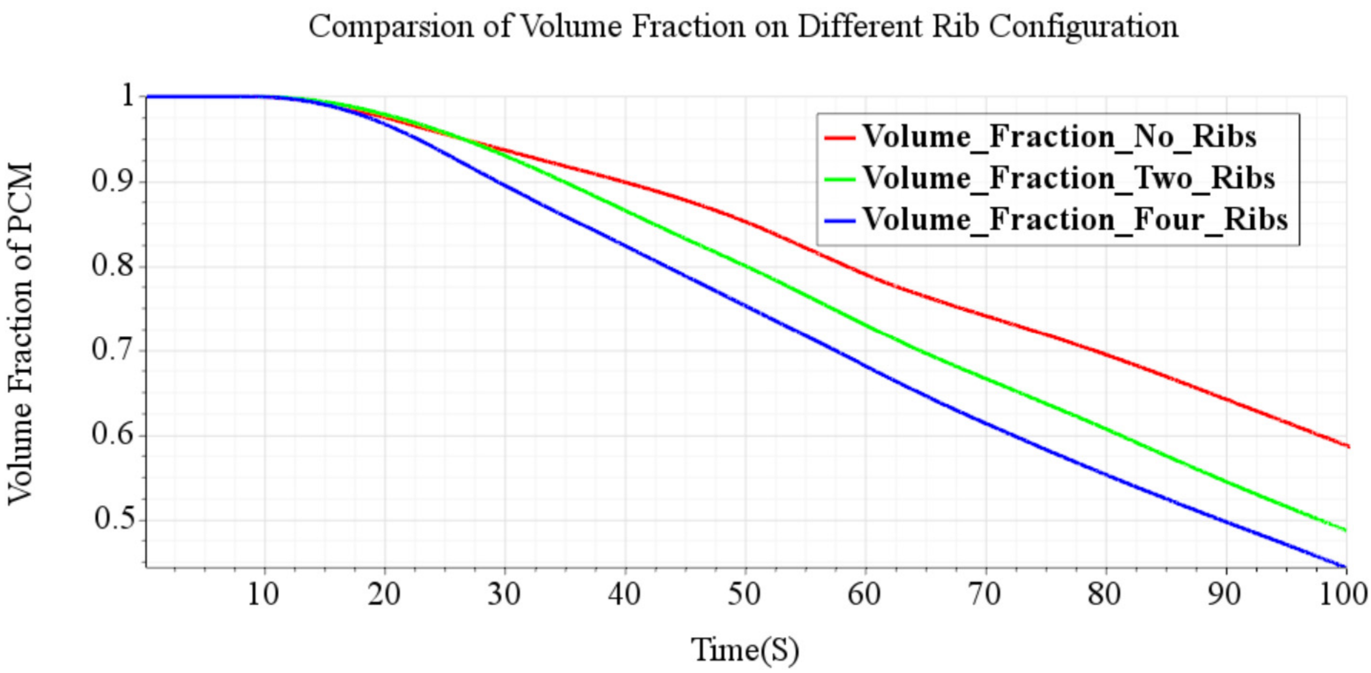

Figure 10. The volume change with function of time for different rib configuration.

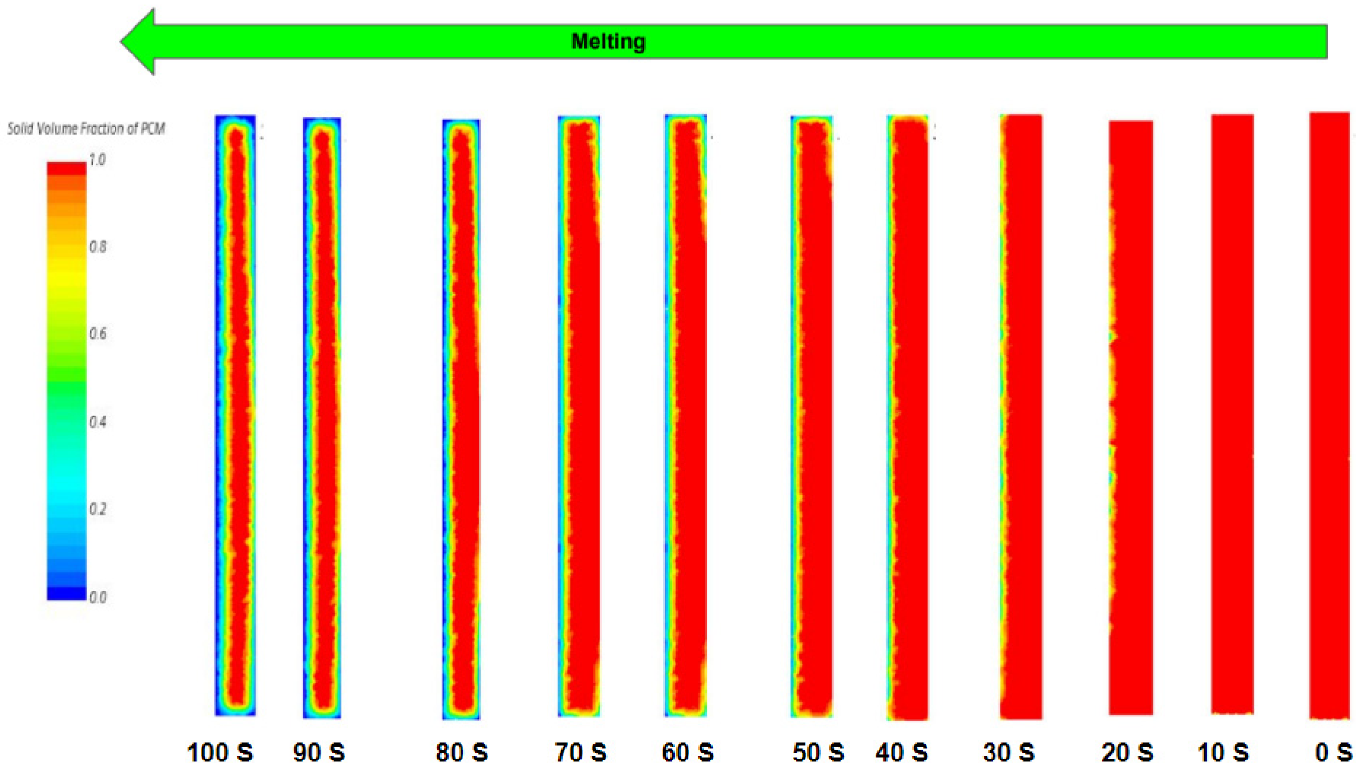

Figure 11. The volume change with function of time for no rib configuration.

The melting process is faster with two rib configurations, as shown in the Figure 12, compared to no rib configurations. There is only a very small change in the PCM material till 20 s. After 30 s, the melting process starts and a visible phase change can be observed in the PCM material. The ribs added between the brackets help to achieve better heat transfer compared to no rib configurations. The phase change continues till 100 s, where the PCM changes phase by 50%. The outer bracket reaches a temperature of 140 °C and helps the outer bracket convert the heat to the surrounding area, which is better than no rib configurations it is based on the Figures 13 and 14.

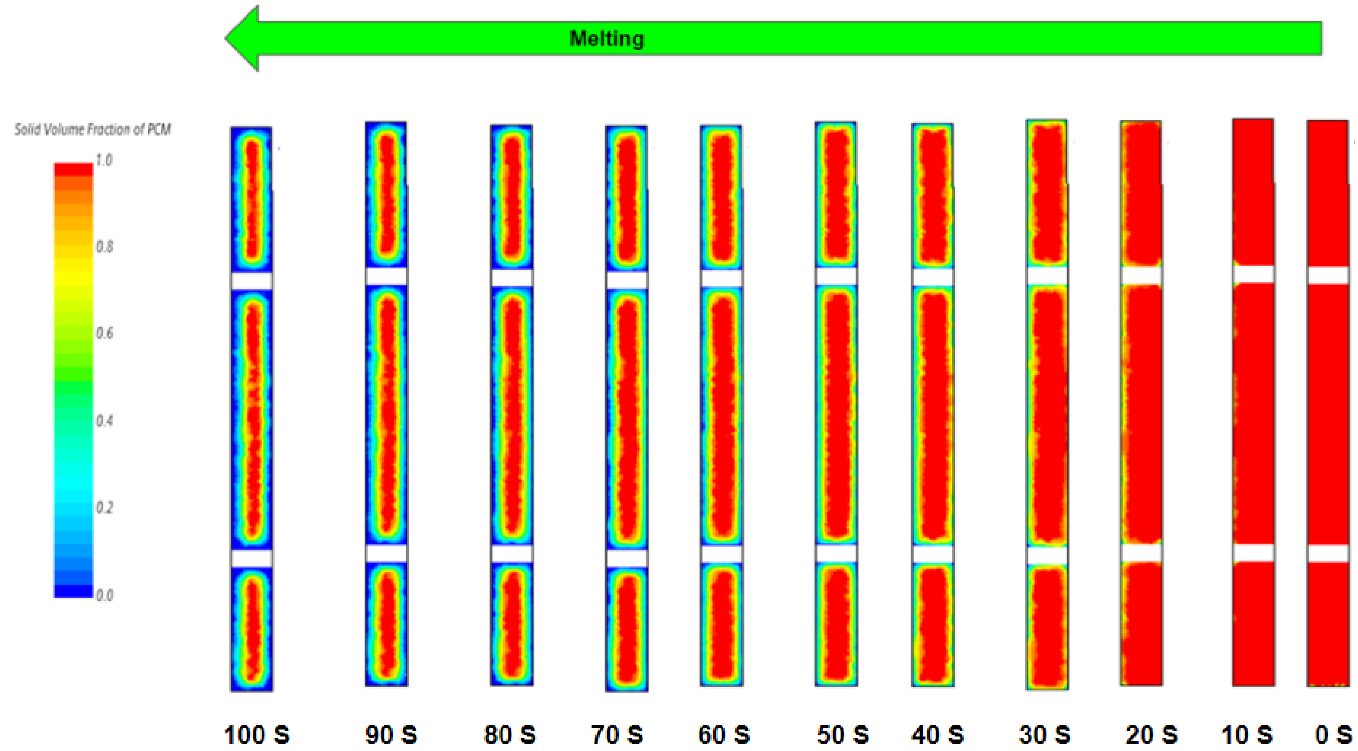

Figure 12. The volume change with function of time for two rib configuration.

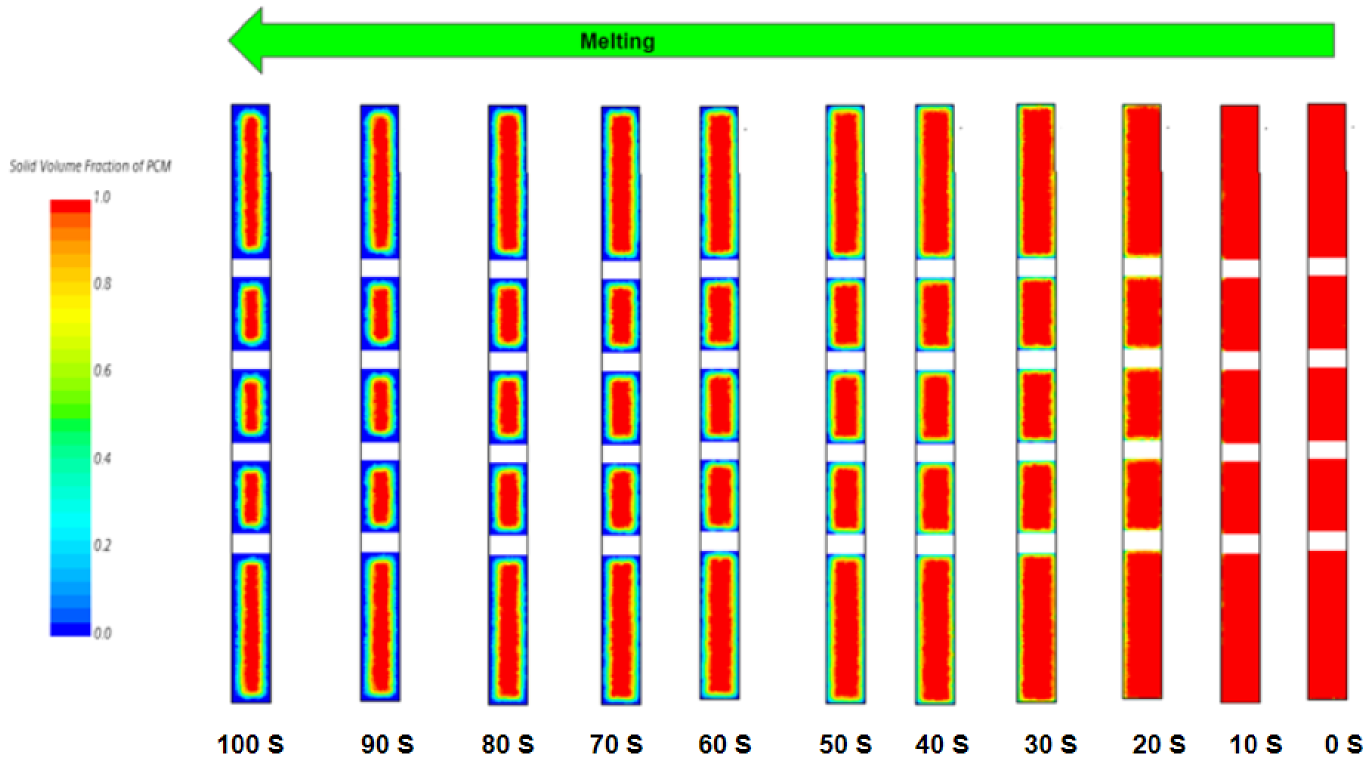

Figure 13. The volume change with function of time for four rib configuration.

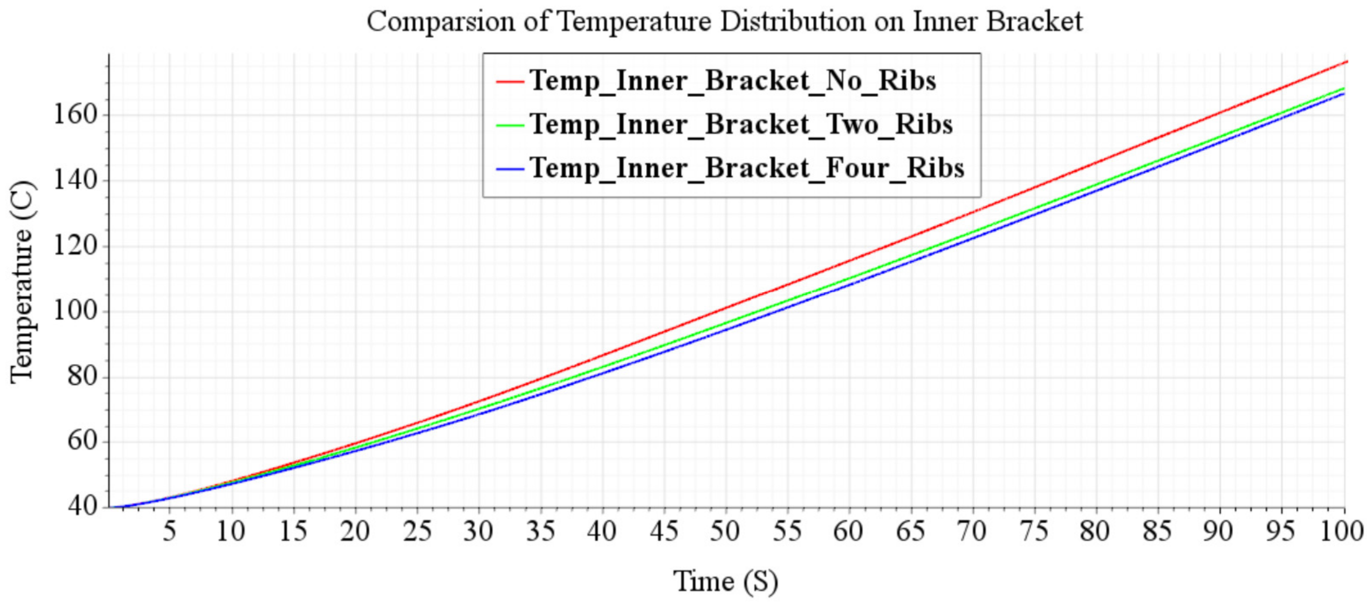

Figure 14. The inner bracket temperature change with function of time for four rib configuration.

The best configuration was observed with four ribs where the temperature distribution and phase change of material were faster compared to other configurations as shown in Figure 13. Based on the results, we can clearly understand that the additional ribs help to have better heat transfer between the outer and inner bracket. After 100 s, the phase change of the material is around 55.5%, which is better than other configurations, as shown in Figure 10. The ribs help the outer bracket to achieve better heat transfer and to move heat out of the system to the surroundings.

6.2. Comparison of Temperature Change for Different Rib Configurations

After 5 s the temperature of the outer bracket reaches 1 °C. For every 5 s the temperature of outer bracket then increases by an additional 2 °C. After 10 s the temperature of four rib configuration is 5 °C. The PCM material changes its phase when the temperature of the bracket reaches 5 °C. The melting of phase change material starts at this point and PCM absorbs heat from the stator and inner bracket. From the Figures 14 and 15 we can clearly note that the four rib configuration has higher heat transfer compared to other configurations. The temperature gradient between the no rib configuration and four rib configuration is around 15 °C. It can be clearly understood that the ribs in between the brackets help to transfer the heat and the PCM absorbs the heat from the stator. The four ribs configuration and two rib configuration follow the same pattern of curve with a temperature difference of 5 °C. The outer bracket is exposed to a convective environment. The heat will transfer to the surroundings, which helps to reach the equilibrium temperature faster.

Along with this, the heat capacity of different rib configurations was compared as shown in Figure 16. The four rib configuration had lower heat capacity when compared with other rib configurations. As we observed, the four rib configuration had a lower temperature difference between the initial and final time of 100 s. The same behaviour is observed in the heat capacity, as shown in Figure 16.

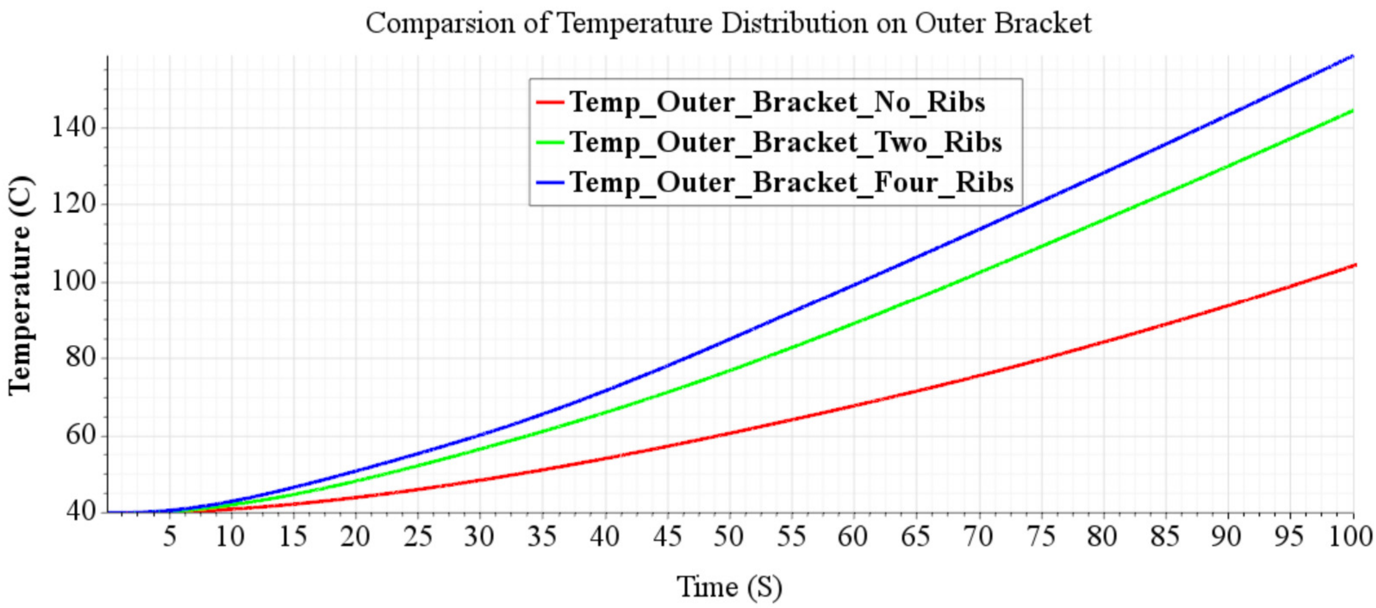

Figure 15. The outer bracket temperature change with function of time for four rib configuration.

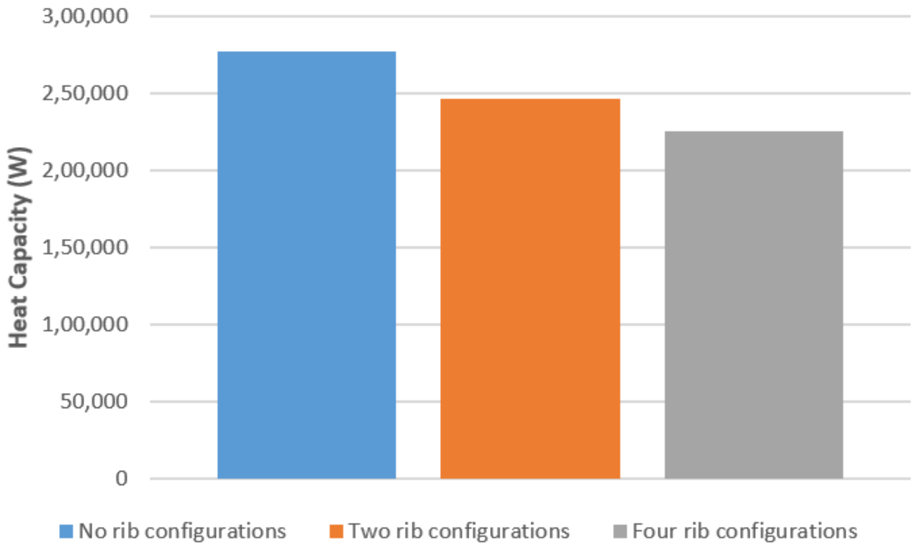

Figure 16. The comparison of heat capacity of different rib configuration.

6.3. Comparison of Two Different PCMs on Four Rib Configuration

Based on a comparison of ribs, it was found that the four rib configuration performs better when compared to other rib configurations. For the comparison study, the simulation was performed for 100 s and it helped to understand the thermal field. Now the four rib configurations are being studied further for the cyclic heat load conditions. The heat load is shown in Figure 17 and it shows that the heat load varied as a function of time and that the simulation ran for 400 s, which is the ideal condition of the motor. Compared with two different PCM materials is shown in Table 3, to understand the cooling performance.

The best performing four rib configuration was used to study the impact on PCM, where the temperature distribution and phase change of material are almost the same with less than 1% difference between them, as shown in Figures 18 and 19. Based on the results, we can clearly understand that the four ribs help to have better heat transfer between the outer and inner bracket during cyclic load conditions. After 100 s, the phase change of the material is around 20%, which is similar when compared with both PCM materials. After 200 s, almost 50% of the PCM material is converted into liquid. At 400 s, the complete PCM is converted into liquid form. As a standalone cooling technique for the bracket, it helps to keep the temperature of static components under the limits; simulation is performed for the worst scenario during ideal rpm. In reality, PCM cooling will be supported by rotor fan cooling and a heat sink to enhance the cooling. But the scope of this paper is limited to bracket cooling using PCM.

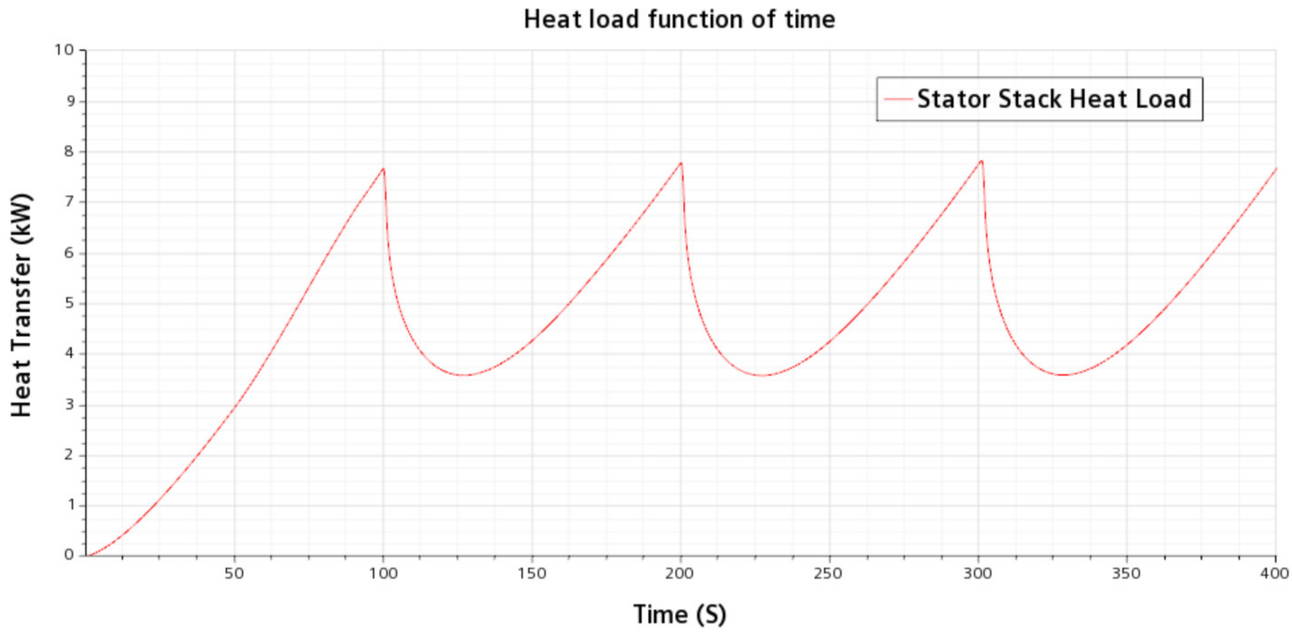

Figure 17. The heat load change with function of time.

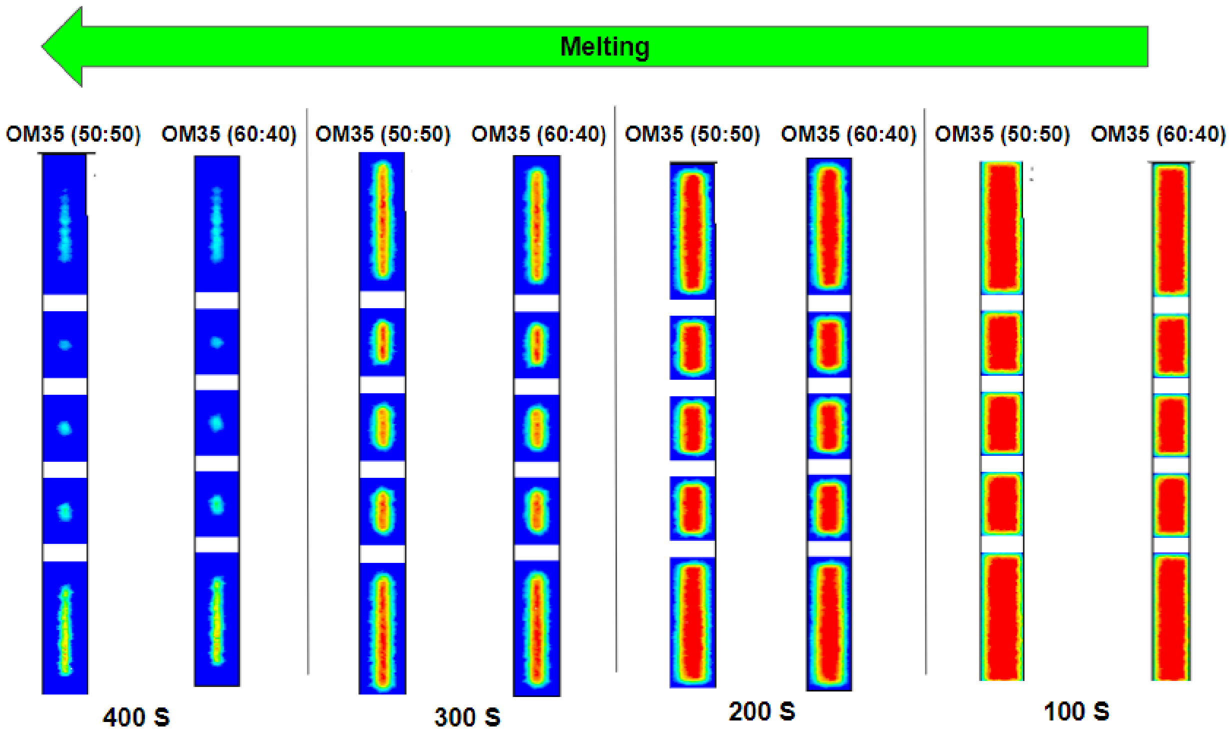

Figure 18. Comparison of volume change with function of time for different PCM materials.

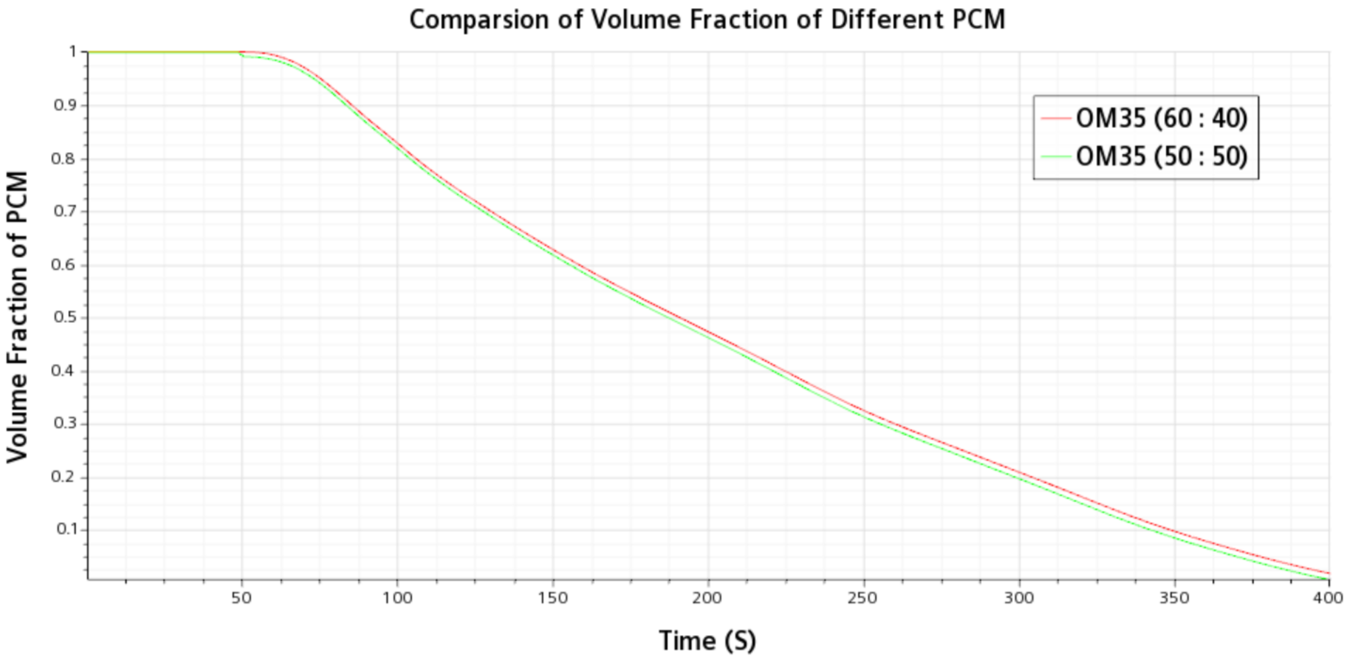

Figure 19. Comparison of volume change plot with function of time for different PCM material.

6.4. Comparison of Temperature Change for Different Rib Configuration

After 50 s, the temperature of the outer bracket reaches 5 °C. The temperature curve becomes linear after 50 s and the increase also becomes linear after that. In the next 50 s, it reaches 20 °C for the cyclic heat load. The behaviour is totally different from the constant heat load condition. The increase is nonlinear for the cyclic heat load conditions. The same holds true for both PCM material combinations. The OM 35 (50:50) performs better compared to the OM 35 (60:40), but the difference in temperature is around 1 °C. A total of four cyclic heat loads are applied and the temperature output of both the inner and outer bracket is plotted in Figures 20 and 21.

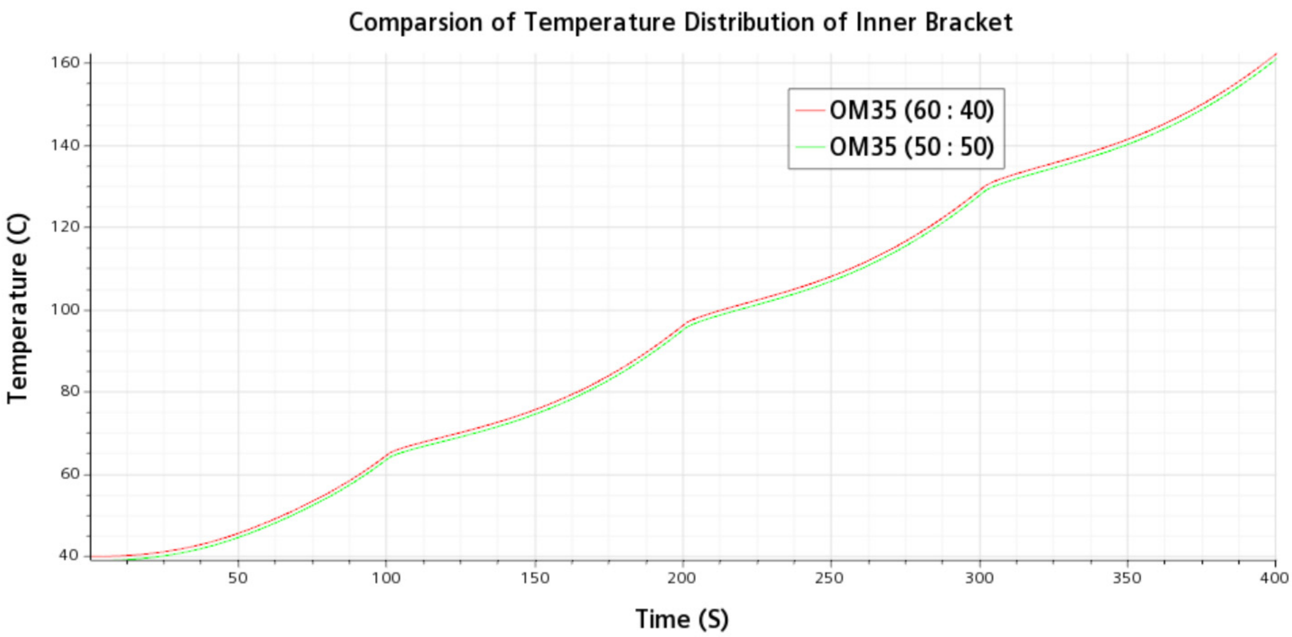

Figure 20. Comparison of temperature distribution of inner bracket plot over time for different PCM materials.

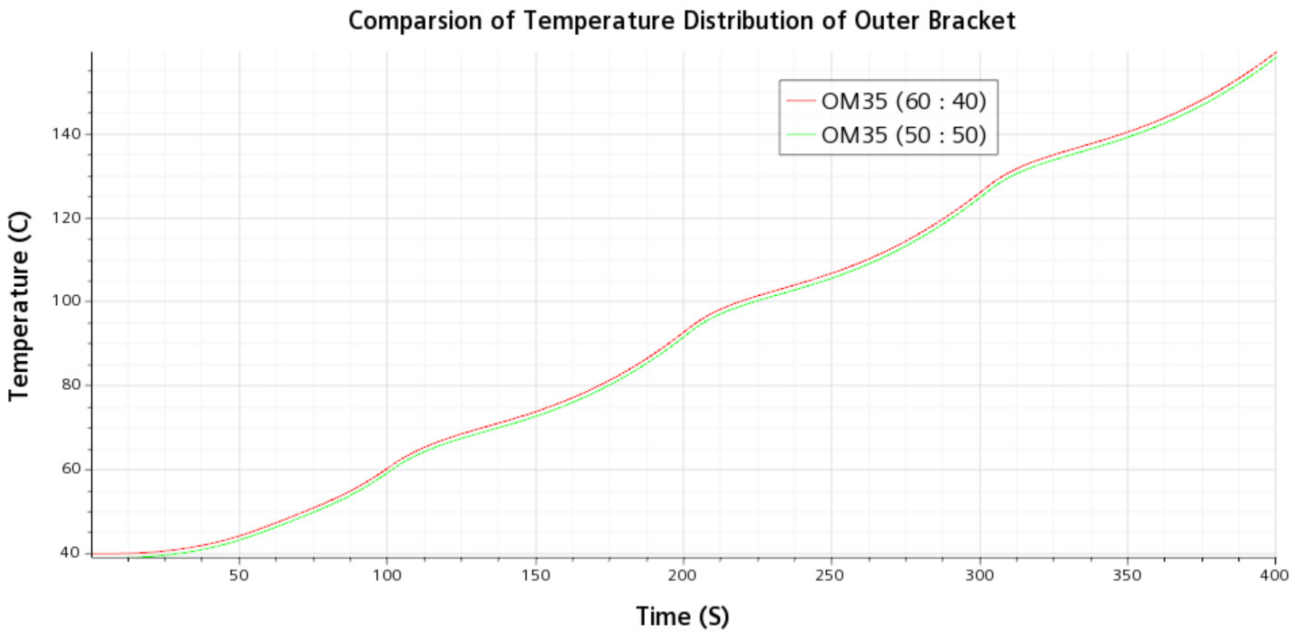

Figure 21. Comparison of temperature distribution of outer bracket plot over time for different PCM material.

7. Conclusions

The arrangement of ribs on the bracket shows that the heat transfer using PCM can be improved by adding more ribs. With an optimum number of ribs, we can achieve better heat transfer. In this research paper the four rib configuration is found to have better heat transfer. The simulation was conducted only for a total time of 100 s, with the aim of understanding the impact of rib configurations. Once the best configurations were known, further studies were conducted using different PCM under cyclic load conditions. We found that an equal combination of OM35 and paraffin gave a better performance in heat transfer. The melting temperature of OM35 had minimal impact ($\leq$1%). Further studies need to be conducted with high thermal conductivity PCM material for better heat transfer. In this study, the horizontal arrangement of ribs was studied. The vertical arrangement along the circumference of the bracket may help to enhance the heat transfer. As of now, the PCM can be used for low voltage applications in a convective environment. For higher voltage applications, PCM along with a secondary cooling passage may help to achieve the cooling requirements.

Author Contributions: Formal analysis, J.S.; investigation, J.S.; methodology, J.S.; software, J.S.; supervision, S.M.; writing—original draft, J.S.; writing—review & editing, S.M. All authors have read and agreed to the published version of the manuscript.

Funding: This research received no external funding.

Conflicts of Interest: The authors declare no conflict of interest.

References

1. Mellor, P.; Roberts, D.; Turner, D. Lumped parameter thermal model for electrical machines of TEFC design. *IEE Proc. B Electr. Power Appl.* **1991**, *138*, 205–218. [CrossRef]
2. Yang, H.; Zhang, H.; Sui, Y.; Yang, C. Numerical analysis and experimental visualization of phase change material melting process for thermal management of cylindrical power battery. *Appl. Therm. Eng.* **2018**, *128*, 489–499. [CrossRef]
3. Sheikholeslami, M.; Haq, R.-U.; Shafee, A.; Li, Z.; Elaraki, Y.G.; Tlili, I. Heat transfer simulation of heat storage unit with nanoparticles and fins through a heat exchanger. *Int. J. Heat Mass Transf.* **2019**, *135*, 470–478. [CrossRef]
4. Matsuzaki, H.; Kimura, Y.; Ohtani, I.; Izumi, M.; Ida, T.; Akita, Y.; Sugimoto, H.; Miki, M.; Kitano, M. An Axial Gap-Type HTS Bulk Synchronous Motor Excited by Pulsed-Field Magnetization With Vortex-Type Armature Copper Windings. *IEEE Trans. Appl. Supercond.* **2005**, *15*, 2222–2225. [CrossRef]

5. Davin, T.; Pellé, J.; Harmand, S.; Yu, R. Experimental study of oil cooling systems for electric motors. *Appl. Therm. Eng.* **2015**, *75*, 1–13. [CrossRef]
6. Lim, D.H.; Kim, S.C. Thermal performance of oil spray cooling system for in-wheel motor in electric vehicles. *Appl. Therm. Eng.* **2014**, *63*, 577–587. [CrossRef]
7. King, J.E.; Kobuck, R.M.; Repp, J.R. High speed water-cooled permanent magnet motor for pulse alternator based pulse power systems. In Proceedings of the 2008 14th Symposium on Electromagnetic Launch Technology, Victoria, BC, Canada, 10–13 June 2008; pp. 1–6.
8. Kim, M.-S.; Lee, K.-S.; Um, S. Numerical investigation and optimization of the thermal performance of a brushless DC motor. *Int. J. Heat Mass Transf.* **2009**, *52*, 1589–1599. [CrossRef]
9. Huang, Z.; Marquez, F.; Alakula, M.; Yuan, J. Characterization and application of forced cooling channels for traction motors in HEVs. In Proceedings of the 2012 XXth International Conference on Electrical Machines, Marseille, France, 2–5 September 2012; pp. 1212–1218.
10. Mudawar, I.; Bharathan, D.; Kelly, K.; Narumanchi, S. Two-Phase Spray Cooling of Hybrid Vehicle Electronics. *IEEE Trans. Components Packag. Technol.* **2009**, *32*, 501–512. [CrossRef]
11. Karim, Z.A.A.; Yusoff, A.H.M. Cooling System for Electric Motor of an Electric Vehicle Propulsion. *Adv. Mater. Res.* **2014**, *903*, 209–214. [CrossRef]
12. Zhang, F.; Song, S.; Du, G.; Li, Y. Analysis of the 3D steady temperature field of MW high speed permanent magnet motor. In Proceedings of the 2013 International Conference on Electrical Machines and Systems (ICEMS), Busan, Korea, 26–29 October 2013; pp. 1351–1354.
13. Camilleri, R.; McCulloch, M. Investigation of an Integrated Evaporative Cooling Mechanism for an Outer-Rotor Permanent Magnet Machine. *Heat Transf. Eng.* **2014**, *36*, 1192–1202. [CrossRef]
14. Woolmer, T.J.; McCulloch, M.D. Analysis of the yokeless and segmented armature machine. In Proceedings of the 2007 IEEE International Electric Machines & Drives Conference, Antalya, Turkey, 3–5 May 2007; Volume 1, pp. 704–708.
15. Lamperth, M.; Beaudet, A.; Jaensch, M. Disc motors for automotive applications. In Proceedings of the Hybrid & Eco Friendly Vehicles Conference 2008 (HEVC 2008), Coventry, UK, 8–9 December 2008. [CrossRef]
16. Liwei, S.; Zijian, L.; Jingyi, G.; Qingchu, Z.; Fuping, W. Thermal effect on water cooling induction motor's performance used for HEV. In Proceedings of the 2008 IEEE Vehicle Power and Propulsion Conference, Harbin, China, 3–5 September 2008; pp. 1–4.
17. Yoon, M.; Jeon, C.; Kauh, S. Efficiency increase of an induction motor by improving cooling performance. *IEEE Trans. Energy Convers.* **2002**, *17*, 1–6. [CrossRef]
18. Odvrka, E.; Shanel, M.; Brown, N.; Narayanan, S.; Ondruek, C.; Mebarki, A. Thermal modelling of water-cooled axial-flux permanent magnet machine. In Proceedings of the 5th IET International Conference on Power Electronics, Machines and Drives (PEMD 2010), Brighton, UK, 19–21 April 2010.
19. Brütsch, R.; Tari, M.; Fröhlich, K.; Weiers, T.; Vogelsang, R. Insulation Failure Mechanisms of Power Generators [Feature Article]. *IEEE Electr. Insul. Mag.* **2008**, *24*, 17–25. [CrossRef]
20. Emanuel, A. A quantitative approach to estimate the life expectancy of motor insulation systems. *IEEE Trans. Dielectr. Electr. Insul.* **2002**, *9*, 627–628. [CrossRef]
21. Borges, S.S.; Cezario, C.A.; Kunz, T.T. Design of water cooled electric motors using CFD and thermography techniques. In Proceedings of the 2008 18th International Conference on Electrical Machines, Vilamoura, Portugal, 6–9 September 2008; pp. 1–6.
22. Kay, J.M.; Nedderman, R.M. *Fluid Mechanics and Transfer Processes*; Cambridge University Press Archive; Cambridge University Press: Cambridge, NY, USA, 1985.
23. Pradeep, R.; Venugopal, T. Experimental study of lithium-ion battery cooling using mixture of phase change materials. *Int. J. Electr. Hybrid Veh.* **2020**, *12*, 168–183. [CrossRef]